Live-Cell Chromosome Dynamics and Outcome of X Chromosome Pairing Events during ES Cell Differentiation

Osamu Masui, Isabelle Bonnet, Patricia Le Baccon, Isabel Brito, Tim Pollex, Niall Murphy, Philippe Hupé, Emmanuel Barillot, Andrew S. Belmont, Edith Heard

Cell

Live-Cell Chromosome Dynamics and Outcome of X Chromosome Pairing Events during ES Cell Differentiation

Osamu Masui,[1,2,3,9] Isabelle Bonnet,[1,2,3] Patricia Le Baccon,[1,4] Isabel Brito,[1,5,6] Tim Pollex,[1,2,3] Niall Murphy,[1,2,3] Philippe Hupé,[1,5,6,7] Emmanuel Barillot,[1,5,6] Andrew S. Belmont,[8] and Edith Heard[1,2,3,*]
[1]Institut Curie, 26 rue d'Ulm, Paris F-75248, France
[2]CNRS UMR3215, Paris F-75248, France
[3]INSERM U934, Paris F-75248, France
[4]CNRS UMR218, Paris F-75248, France
[5]INSERM U900, Paris F-75248, France
[6]Mines ParisTech, Fontainebleau F-77300, France
[7]CNRS UMR144, Paris F-75248, France
[8]Department of Cell and Developmental Biology, University of Illinois, 601 South Goodwin Avenue, Urbana, IL 61801, USA
[9]Present address: Research Centre for Allergy and Immunology, RIKEN Yokohama Institute, 1-7-22, Suehiro-cho, Tsurumi, Yokohama, Kanagawa 230-0045, Japan
*Correspondence: edith.heard@curie.fr
DOI 10.1016/j.cell.2011.03.032

SUMMARY

Random X inactivation represents a paradigm for monoallelic gene regulation during early ES cell differentiation. In mice, the choice of X chromosome to inactivate in XX cells is ensured by monoallelic regulation of *Xist* RNA via its antisense transcription unit *Tsix*/*Xite*. Homologous pairing events have been proposed to underlie asymmetric *Tsix* expression, but direct evidence has been lacking owing to their dynamic and transient nature. Here we investigate the live-cell dynamics and outcome of *Tsix* pairing in differentiating mouse ES cells. We find an overall increase in genome dynamics including the Xics during early differentiation. During pairing, however, Xic loci show markedly reduced movements. Upon separation, *Tsix* expression becomes transiently monoallelic, providing a window of opportunity for monoallelic *Xist* upregulation. Our findings reveal the spatiotemporal choreography of the X chromosomes during early differentiation and indicate a direct role for pairing in facilitating symmetry-breaking and monoallelic regulation of *Xist* during random X inactivation.

INTRODUCTION

X chromosome inactivation (XCI) ensures equal levels of X-linked gene products in females (XX) and males (XY) (Lyon, 1961). XCI is initiated during early development via upregulation of the noncoding *Xist* transcript, which coats one X chromosome in *cis* and triggers its silencing. Once established, XCI is then maintained through propagation of epigenetic marks during cell divisions. A remarkable feature of XCI is that two identical chromosomes become differentially expressed in the same nucleoplasm. Germline imprinting provides one way of achieving asymmetric expression (see Okamoto and Heard, 2009 for review). However, in most eutherians, and in postimplantation mouse embryos, XCI is random, with either the paternal or maternal X being silenced (Lyon, 1961). Random monoallelic gene expression has also been reported to occur at some autosomal loci, with potentially important implications for development and disease (Gimelbrant et al., 2007).

In the case of random XCI, the X-inactivation center (Xic), which includes the *Xist* gene and its antisense transcript *Tsix*, controls the initiation of this process (see Navarro and Avner, 2010 for review). XCI takes place during the earliest stages of embryonic stem (ES) cell differentiation, at a time when other important developmental decisions are also being made. In undifferentiated female ES cells, *Xist* and *Tsix* are expressed at low levels, but upon differentiation, *Xist* becomes upregulated and *Tsix* downregulated on one of the two X chromosomes (Lee et al., 1999; Debrand et al., 1999). Consistent with this inverse expression pattern, *Tsix* and its enhancer *Xite* (Lee et al., 1999; Lee and Lu, 1999, Sado et al., 2001; Ogawa and Lee, 2003) are known to repress *Xist* in *cis*.

Understanding how *Xist* becomes asymmetrically upregulated during early differentiation is thus central to our understanding of how the two X chromosomes become differentially expressed during random XCI. Activation of *Xist* during ES cell differentiation depends on downregulation of pluripotency factors such as Oct4, Nanog, and Sox2 (Navarro et al., 2008), as well as the presence of XX-dosage-sensitive competence of sensing factors, such as the X-linked Rnf12 protein (Jonkers et al., 2009), and possibly other loci (*Xpr*) or noncoding transcripts (*Jpx*, *Ftx*) located 5′ to *Xist* (Augui et al., 2007; Tian et al., 2010; Chureau et al., 2011). However, these sensing mechanisms do not readily explain why only one of the two *Xist* alleles is

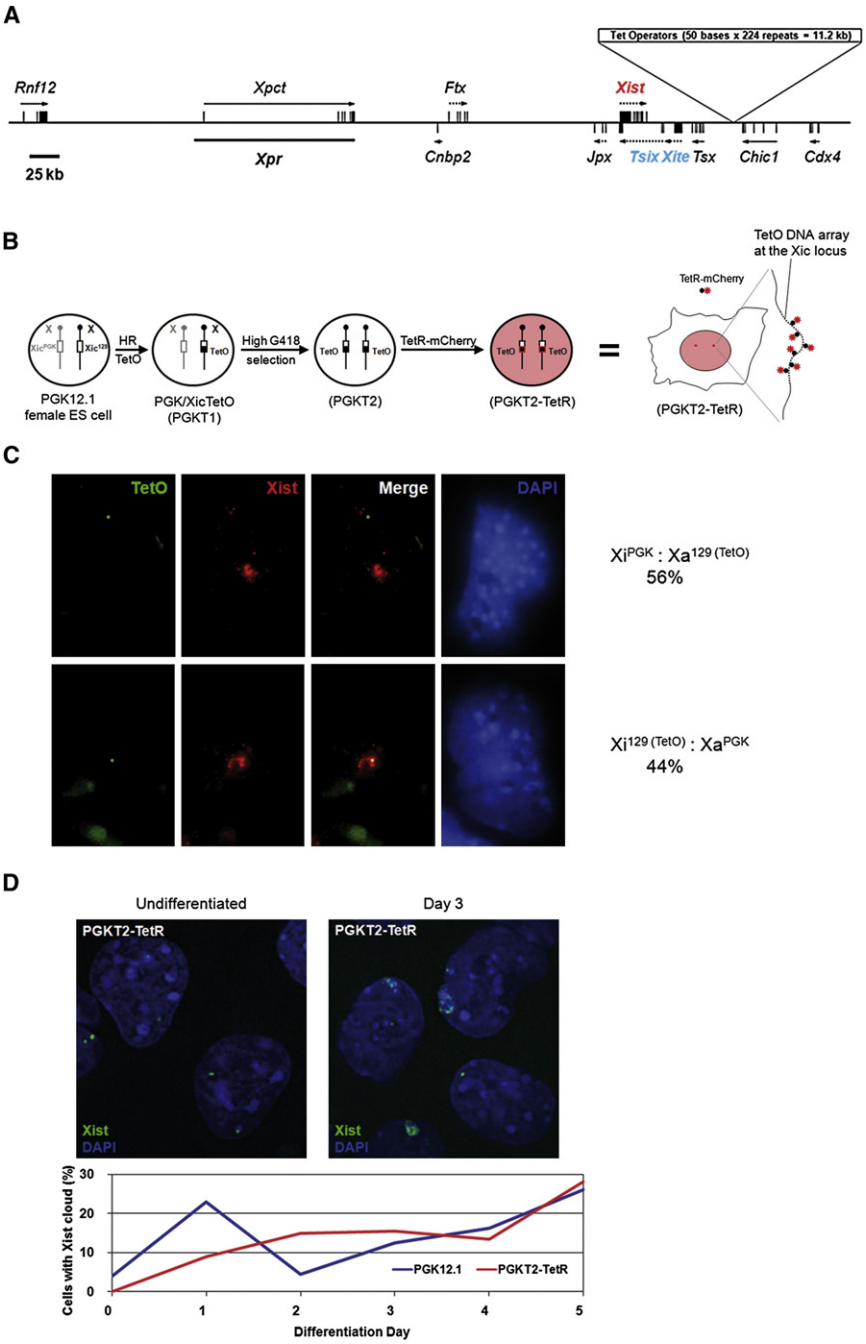

Figure 1. Generation of Xic^{TetO} Homozygous Female ES Cells

(A) A map of the Xic locus and the position of the TetO integration is indicated. Arrows indicate the transcription direction of each gene. Broken lines represent putative noncoding transcripts.

(B) Schematic representation of the strategy used to generate PGKT2-TetR cells. The TetO array can be bound by TetR-mCherry and used to visualize the locus in living cells.

(C) DNA/RNA FISH for TetO (DNA FISH, green) and *Xist* (RNA FISH, red) on PGKT1 cells at day 5 of differentiation. Upper panels: *Xist* RNA accumulates on non-TetO-targeted X chromosome. Lower panels: *Xist* accumulates on TetO-targeted X chromosome (n = 64).

(D) Kinetics of *Xist* RNA accumulation in parental PGK12.1 cells and in the TetO-targeted PGKT2-TetR cells (n > 100 per day of differentiation). Representative pictures for undifferentiated and day 3 differentiated PGKT2-TetR cells are indicated (green, *Xist* RNA).

See also Figure S1.

upregulated, not both. Stochastic *Xist* expression models might partly explain this (Monkhorst et al., 2008), but the surprisingly low frequency of biallelic *Xist* upregulation during the initiation of XCI in mice suggests that some other means of ensuring precise monoallelic regulation exists.

Recently it was shown that the two Xic loci undergo transient homologous associations (pairing) during early differentiation, and it was proposed that this might play a role in the monoallelic regulation of *Xist* and *Tsix* during initiation of XCI (Bacher et al., 2006; Xu et al., 2006, 2007; Augui et al., 2007). Associations between homologous chromosomal loci have been proposed to underlie the establishment of opposite states of transcriptional activity on homologous alleles in other situations, for example, during immunoglobulin recombination in B cell development (Hewitt et al., 2009). In the case of X inactivation, pairing via the *Xpr* locus (Figure 1A) has been proposed to help bring together and facilitate pairing at the *Tsix* loci (Augui et al., 2007), which in turn is proposed to enable coordination of monoallelic *Tsix* expression and reciprocal *Xist* expression (Xu et al., 2007; Scialdone and Nicodemi, 2008). In support of this, deletion of both alleles of *Tsix* in females results in chaotic XCI, with biallelic or no *Xist* upregulation in a significant proportion of cells (Lee, 2005). However, the coordinating role of *Tsix* pairing in monoallelic XCI has never been tested experimentally, and the actual relationship between Xic pairing and *Xist*/*Tsix* regulation has remained unclear, partly because of the asynchronous nature and heterogeneity of early differentiating ES cells, which renders the precise ordering of events impossible in fixed cells, where only snapshots of dynamic events can be obtained.

In this paper, we set out to examine the dynamics of X chromosome pairing and its possible outcome, using the Tet operator/Tet repressor (TetO/TetR) tagging system in living ES cells. Both the Xic loci as well as other autosomal regions were visualized in real time in this way. We find a general increase in the

dynamics of loci during early ES cell differentiation. This could have important implications for the multiple developmental decisions being taken during this time. We show that *Tsix* pairing is a transient event, lasting approximately 45 min, and that during pairing, the *Tsix* loci show reduced mobility, suggesting some form of tethering to each other. We also demonstrate that the outcome of pairing is often monoallelic *Tsix* expression, which could in turn lead to monoallelic *Xist* upregulation. We thus present one of the first live-cell investigations of the dynamics of genomic loci during early XX ES cell differentiation and demonstrate that transient homologous associations can provide an efficient means of generating asymmetric expression states.

RESULTS

Generation of TetO-Tagged Xic Loci in Female ES Cells

To visualize the Xic loci and other genomic loci in living ES cells, we exploited the TetO/TetR system (Michaelis et al., 1997). We first targeted a single TetO array into a site located 65 kb downstream of *Xist*'s 3′ end and 35 kb away from *Xite* (Figure 1A and Figure S1A available online), in order to avoid any deleterious effects on *Xist*/*Tsix*/*Xite* regulation and initiation of XCI. The homologous recombination construct harboring the 224-repeat TetO array (11.2 kb) and a neomycin resistance gene was targeted into one of the two Xic loci in the PGK12.1 mouse female ES cell line (Penny et al., 1996) (Figure 1B and Figure S1A). Two correctly targeted clones out of 310 screened were obtained and one of them was used for further analysis (Figure S1B).

Insertion of the TetO into the Xic did not affect the onset of XCI or the choice of X chromosome for XCI. The hemizygous clone (PGKT1) was differentiated in vitro and analyzed for random XCI by *Xist* RNA FISH accompanied by TetO DNA FISH to distinguish the TetO-tagged allele. Normal kinetics of *Xist* upregulation and similar frequencies of XCI were observed for both the Xic^{TetO} and untagged Xic alleles (Figure 1C and data not shown).

This hemizygous PGKT1 clone was then used to generate ES cells in which both Xic loci were tagged for visualization. Initially, targeting of the second Xic locus was attempted using a targeting construct containing a Lac operator (LacO) array. However, this failed despite repeated attempts. Instead, we generated Xic^{TetO} homozygous cells by treating the hemizygous PGKT1 cells using increased G418 selection (Figure 1B) (Mortensen et al., 1992). One of the clones obtained (PGKT2) was found to have two X chromosomes, each of which carried a TetO-tagged Xic locus based on Southern blotting and DNA FISH on metaphase spreads (Figures S1B–S1D). A TetR-mCherry fusion protein construct was introduced into the PGKT2 cell line as a stable transgene to enable visualization of the two Xic^{TetO} loci (Figure 1B). In this clone (PGKT2-TetR), two TetR-mCherry foci could be readily detected by fluorescence microscopy (Figure S1E and Movie S1). The two TetR-mCherry foci corresponded to the TetO-tagged Xics as they systematically colocalized with punctate *Xist*/*Tsix* RNA FISH signals in undifferentiated ES cells (Figure S1E). Upon differentiation of PGKT2-TetR cells, monoallelic *Xist* RNA accumulation was observed with similar kinetics to the parental line (Figure 1D). We conclude that the presence of the TetO tag within each of the Xic loci and the expression of the TetR-mCherry protein in PGKT2-TetR cells did not interfere with normal XCI induction and kinetics. The PGKT2-TetR cell line was therefore used for subsequent experiments. In the course of this work, we also generated a series of ES cell lines carrying randomly inserted, autosomal TetO arrays, which we were able to use to assess general chromosome mobility, as will be described later.

Detection of Xic^{TetO} Pairing in Living ES Cells

We next established conditions for live-cell imaging of TetO-tagged Xic loci in PGKT2-TetR ES cells (Figure S2A; see also Experimental Procedures). Following deconvolution of three-dimensional (3D) image stacks, more than 80% of nuclei showed two clear Xic^{TetO} spots. In some cases, the TetR-bound locus appeared as a doublet, presumably due to sister chromatid separation (Figure 2A and Movie S1 and Movie S2). In order to determine the time window in which Xic pairing most often occurred, we assessed Xic pairing frequencies at different stages of differentiation, by measuring 3D distances between the centers of mass of the two Xic^{TetO} spots in snapshots of living cells (Figures 2A and 2B). Based on our previous criteria defined in fixed cells, pairing in living cells was defined as Xic-Xic distances of ≤ 2 μm (Augui et al., 2007). A peak in Xic^{TetO} pairing frequencies was found at day 1 of differentiation, as indicated by a marked shift to shorter TetO-TetO distances when compared to undifferentiated cells or late differentiated cells (day 8) (Figures 2B and 2C and Figure S2B). We reproducibly observed a peak of approximately 5% to 10% cells showing Xic^{TetO} pairing at around day 1 of differentiation in three independent experiments (Figures 2B and 2C and data not shown). These results agree with previous DNA FISH studies, where *Tsix* pairing was significantly enriched at day 1 or 2 of differentiation (Bacher et al., 2006; Augui et al., 2007), and show that TetO-tagging of Xic loci does not interfere with normal pairing kinetics.

Increased Mobility of the Xics and Other Genomic Loci during ES Cell Differentiation

In order to determine the general context in which Xic pairing events occur, we wished to assess the dynamics of the Xics and of other genomic loci during ES cell differentiation. First, time-lapse 3D imaging was performed at various stages of differentiation of PGKT2-TetR cells (Figure 2A). Using imaging conditions that minimize phototoxicity in differentiating ES cells (see Experimental Procedures), we first carried out experiments using 1 min time intervals ($\Delta t = 1$ min), over a 30 min period, in undifferentiated and differentiated ES cells (from days 1 to 4) (illustrated in Movie S1 for undifferentiated cells and Movie S2 for day 1 differentiated cells). The distances (d) between two loci were used to assess mobility, as this avoids issues of nuclear rotation (Marshall et al., 1997). Measuring 3D distances at each time point ($n > 50$ cells imaged, at each day of differentiation), we noted that distances between the two Xic^{TetO} loci appeared to be more variable during early differentiation as compared to undifferentiated ES cells, indicating a possible increase in mobility. This is illustrated when the change in TetO-TetO distances is plotted over time for multiple cells (Figure S2C, compare cells differentiated for 1 or 2 days to undifferentiated cells).

To quantify whether there was a difference in mobility and assess whether the movements observed were random

A

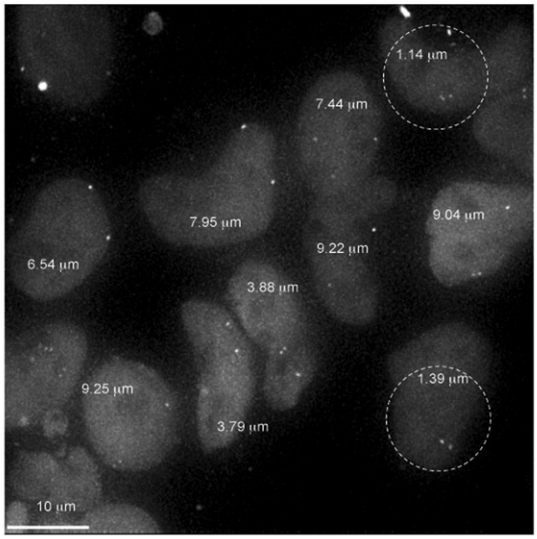

B

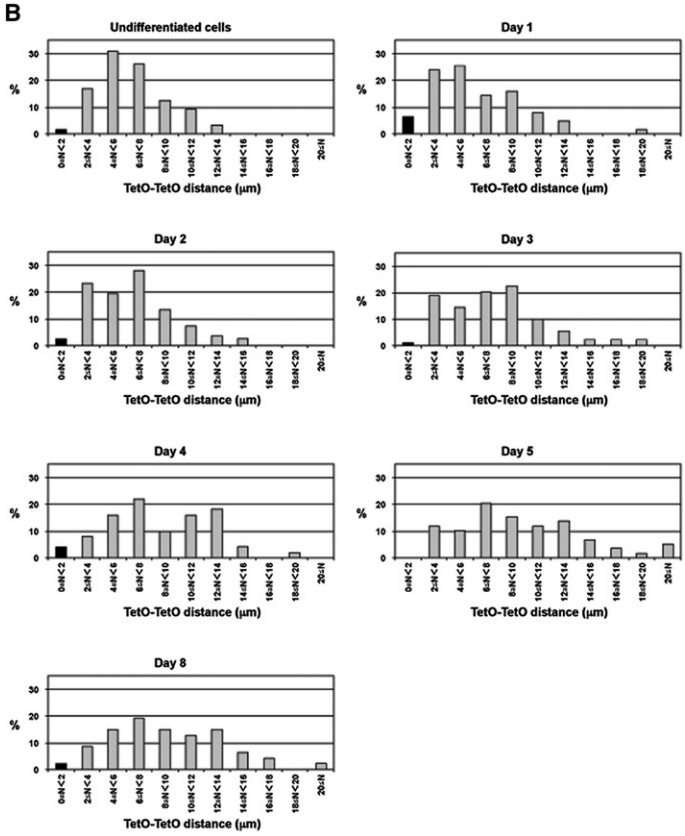

C

	Average d (μm)	Median d (μm)	d ≤ 2 μm	n
Undiff. Cells	6.5 ± 2.7	6.3	1.5%	65
Day 1	6.2 ± 3.5	5.4	6.3%	63
Day 2	6.6 ± 3.1	6.3	2.4%	82
Day 3	7.7 ± 3.8	7.5	1.1%	89
Day 4	8.5 ± 3.9	8.1	4.0%	50
Day 5	9.9 ± 5.1	8.6	0.0%	59
Day 8	9.2 ± 4.5	8.5	2.1%	47

Figure 2. Analysis of Xic^{TetO} Dynamics by Live-Cell Imaging

(A) An example of a projected deconvolved image of day 1 differentiated living PGKT2-TetR cells. Indicated values correspond to the 3D distance between two Xic^{TetO} spots. Xic pairing cells are marked with white circles.

(B) Detailed distribution of 3D distances between two Xic^{TetO} spots for each differentiation stage shown in (C). The black solid bars indicate the "Xic pairing" population (d $\leq$ 2 μm).

(C) Summary of distribution of 3D distances between two Xic^{TetO} spots for each differentiation stage shown in (B).

See also Figure S2.

(diffusive) or directional, we plotted the mean square displacement (MSD, $< \Delta d^2 >$) of the loci over time (Marshall et al., 1997; Carmo-Fonseca et al., 2002). The slope of the MSD is proportional to the diffusion coefficient (D) of the loci (see Experimental Procedures). The more mobile two loci are, the faster the $< \Delta d^2 >$ value increases over time, and the steeper the MSD slope. We measured the MSD for $\geq$40 cells at each stage of differentiation. For short time experiments, a linear increase of $< \Delta d^2 >$ with increasing time intervals (Δt) was observed in all cases, suggesting that Xic^{TetO} loci undergo diffusive rather than directional motion over a timescale of several to tens of minutes (Figure 3A). However, the MSD $< \Delta d^2 >$ value increased more rapidly in differentiating cells (days 1, 2, 3, and 4) compared to undifferentiated cells (Figure 3A). This increased mobility could be seen even in day 8 differentiated cells (data not shown). At day 1 of differentiation, 47% of cells (n = 62) showed a change in TetO-TetO distances of >2 μm over 1 hr, in contrast to only 14% of undifferentiated cells (n = 21). MSD values calculated from data points near the beginning versus the ends of extended observation periods did not change in any significant way indicating that the observed increase in mobility was not due to variable phototoxicity effects in differentiated versus undifferentiated cells (Figure S3A). We could also exclude that this increase in mobility was due to increased nuclear volume during differentiation, as we found no significant change in nuclear volume in day 1 differentiated cells compared to undifferentiated cells (data not shown), similarly to a previous study (Bacher et al., 2006), even though mobility changed substantially between these two time points. At sufficiently longer times, the plateau of an MSD curve reflects constraints on long-range chromatin mobility imposed by chromosome and/or nuclear structure (see legend to Figure 3B). Measurements over longer time periods ($\geq$120 min) revealed radii of "constrained diffusion" of ~1.7 μm (square root of 3 μm^2 plateau) for both days 0 and 1. This is in the range of chromosome territory size and well below nuclear size (Figure 3B).

We next evaluated whether the increase in mobility we observed during early differentiation was specific to the Xic locus

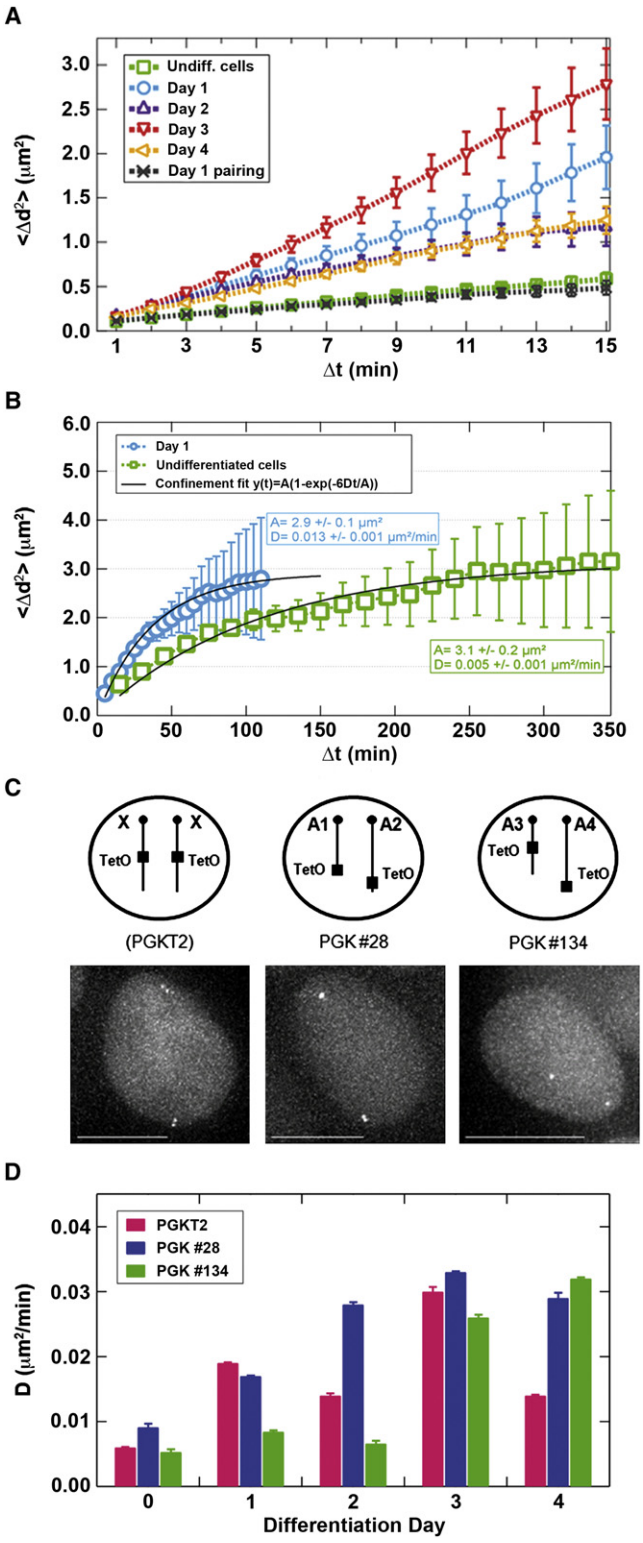

Figure 3. Analysis of Xic^{TetO} Mobility in Living ES Cells

(A) Averaged mean square displacement curves (MSD, $< \Delta d^2 >$) calculated from changes in distance between two Xic^{TetO} spots for cells at different stages of differentiation. MSDs were derived from experiments at Δt = 1 min time intervals, for a total of 30 min, and averaging was done over all the analyzed cells. For each time point, the statistical error after averaging over N cells (see Experimental Procedures for details) is plotted as the error bar (day 0, N = 82; day 1, N = 45; day 2, N = 47; day 3, N = 47; day 4, N = 57; and day 1 pairing cells, N = 44). MSD curves depend linearly on time, which demonstrate the relative diffusive motion of the two Xic^{TetO} spots. The MSDs for undifferentiated cells (green) and day1 pairing cells (gray) are similar, whereas a significant increase of the MSD slope is observed for differentiated cells.

(B) Averaged MSD curves for long time-lapse experiments to see confinement effect. Green squares: MSD for undifferentiated cells (N = 44) derived from movies of 450 min duration with 15 min interval time. Blue circles: MSD for differentiated cells (N = 26) at day 1 of differentiation calculated from movies of 150 min with 5 min intervals. Error bars are the same as in (A). Characteristic confinement area A is determined by fitting (black lines) the experimental MSD points to the expression for a confined motion: $<\Delta d^2> = A \times (1 - e^{-6Dt/A})$. Typical area of confinement is around 3 μm^2 for both undifferentiated cells and day 1 differentiated cells, leading to a typical radius of confinement of $\sqrt{3} \approx 1.7 \mu m$. The fit yields D values in excellent agreement with those previously determined by MSD slopes for short-time experiment (see Figure 3D). Because $D_{undiff.\ cells}$ is smaller than D_{day1}, the plateau is reached earlier for day 1 differentiated cells (around 95 min) than for undifferentiated cells (around 250 min).

(C) Schematic representation of Xic^{TetO} homozygous line (PGKT2) and two autosomal TetO clones, PGK #28 and PGK #134. Relative positions of TetO integration sites were determined by TetO DNA FISH on metaphase spreads of chromosomes. Photographs are snapshots of live-cell imaging. Scale bar = 10 μm.

(D) Three-dimensional diffusion constant D as a function of differentiation days for the three cell lines shown in (C). D values were deduced from the linear fit of the averaged MSD curves shown in (A). Bars represent the standard deviation of the error provided by the polynomial fitting software.

See also Figure S3 and Movie S3.

or was a more general feature of the genome in early differentiating ES cells. To this end, different ES cell lines in which two independent autosomal loci had been tagged by random integration of TetO arrays and also expressed a TetR-mCherry transgene to enable visualization, were examined (Figure 3C and Movie S3). The TetO-TetO distances in these lines (PGK28 and PGK134) were measured in living cells (in 3D, over time) at different stages of differentiation ($n \geq 39$ cells for each differentiation day) and MSDs were calculated. We observed a general increase in locus mobility upon differentiation, similar to that observed for the Xics, in both cell lines (Figure 3D). Although the kinetics of this increase differed in each case, the trend was the same, implying a general increase in genome mobility during early differentiation. In the case of the Xics, this greater mobility during early differentiation might facilitate the onset of homologous Xic pairing through an increase in the frequency of collisions between loci. On the other hand, it might also inhibit prolonged interactions during pairing. We therefore examined the dynamics of Xic loci during the pairing process in more detail.

Live-Cell Imaging and Dynamics of Xic^{TetO} Pairing

Based on previous fixed cell data, it has remained unclear whether Xic pairing is a transient but frequent event, or else a prolonged but rare event. To assess the frequency and duration of pairing, and the mobility of the Xic loci during this process, live-cell imaging experiments were performed on PGKT2-TetR cells at day 1 of differentiation, which show the highest frequencies of Xic pairing (Figures 2B and 2C). This also corresponds to the time when reciprocal *Xist/Tsix* expression patterns

are first seen. Time-lapse imaging was performed on cells for 30 min periods, with 1 min intervals. We noted that in the majority of cells where Xic pairing (distances $\leq$ 2 μm) was detected, both Xic^{TetO} loci showed separated sister chromatids (84.1%, n = 44) in at least one frame of the 30 min time-lapse movie. Repeated overlap and separation between sister chromatids could be seen on the minute timescale (for example, Movie S1and Movie S4). The detection of sister chromatids at both loci implies that DNA replication must have been completed prior to Xic pairing. Indeed, this is consistent with our previous DNA FISH studies on FACS-sorted cells (Augui et al., 2007), where we found that pairing occurs in S phase after Xic DNA replication. To assess Xic mobility during pairing, we calculated the MSD of the loci in cells displaying Xic distances of less than 2 μm. As shown in Figure 3A and Figure S3B, Xic^{TetO} loci in cells where pairing is ongoing have a remarkably reduced range of movement compared to the total population at day 1 of differentiation. Thus, once the two Xics encounter each other and pairing initiates, the loci become restrained, even in the context of a general increase in mobility during early differentiation. The reduced mobility of the loci observed during pairing would suggest that they may be tethered either to each other or to a common nuclear compartment that provides an additional restraint to that of each polymer to its chromosome.

We also assessed whether Xic^{TetO} loci ever showed complete overlap (i.e., d = 0 μm) during the course of pairing (i.e., d $\leq$ 2 μm). In experiments where 1 min time intervals were used during imaging, the loci did show occasional complete overlap (6.8%, n = 44), although this lasted for only a few minutes at a time (Figure 4A and Movie S4) and was not seen in all cells. Given the transient nature of the overlap, it may actually occur more frequently but would not be captured with the imaging intervals we used.

In order to measure the actual duration of Xic pairing events (d $\leq$ 2 μm), we performed time-lapse experiments for $\geq$150 min, with 5 min intervals to minimize phototoxicity and maintain total light exposure times the same as in 30 min movies. Under these imaging conditions, the cells appeared to grow and divide similarly to cells grown without imaging. Based on analysis of multiple nuclei (n = 8) over 150 min, Xic^{TetO} pairing was found to last an average of 42 min (±31 min), consistent with previous estimates based on fixed cell studies (Xu et al., 2007). A representative cell, filmed for a 150 min period during which the Xic loci come together and remain within 2 μm of each other for 40 min, before separating again, is shown in Figure 4B and Movie S5. A few cells showed loci that appeared to be paired for $\geq$150 min probably corresponding to arrested/dying cells due to the normal process of differentiation, and we did not include them in our analysis. Although longer time-lapse experiments (12–15 hr) were attempted, these were difficult to analyze owing to phototoxicity, as well as the fact that cells would often move out of the field of imaging.

Our previous work has shown that pairing is restricted to early S phase of the cell cycle (Augui et al., 2007), but this does not account for its developmentally restricted onset. Recent studies have suggested that the pluripotency factor Oct4 may play a role in pairing (Donohoe et al., 2009). To assess whether levels of Oct4, or other pluripotency factors that decrease during early differentiation, were correlated with the onset of Xic pairing, we performed immunofluorescence for Oct4 and Nanog following live-cell imaging. No clear-cut correlation could be seen of Oct4 or Nanog levels in Xic pairing versus nonpairing cells (Figure S4), suggesting that overall levels of such factors do not dictate the onset of pairing during differentiation or in the cell cycle.

In conclusion, we find that Xic pairing occurs most frequently at day 1 of differentiation, shows no obvious correlation with pluripotency factor levels, and is a transient event, probably occurring in most of the population at least once per cell cycle during early differentiation. This latter conclusion is based on the fact that Xic pairing lasts for about 45 min on average, which represents approximately 5% of the cell cycle (estimated to be around 15 hr). This number is very close to the frequency observed for Xic pairing in the cell population (approximately 6%) at this stage of differentiation (Figures 2B and 2C). As pairing occurs almost exclusively in early S phase, after DNA replication of the loci (Augui et al., 2007), cell-cycle regulation is likely to account for its transient nature. Finally, the reduced Xic mobility observed during pairing, despite the generalized increase in mobility during early differentiation, indicates that the two loci are somehow tethered, either to each other or to a common nuclear structure during this time.

Demonstration that Xic Pairing Frequently Results in Asymmetric *Tsix* Expression

We next investigated how Xic pairing events might be linked to *Xist*/*Tsix* regulation and the onset of random XCI. In undifferentiated XX ES cells, previous studies have shown that *Tsix* is expressed from both alleles in almost 100% of cells, and *Xist* expression is low (Debrand et al., 1999; Sun et al., 2006). Upon differentiation, *Tsix* is downregulated and *Xist* is upregulated on one of the two X chromosomes during early differentiation (days 1–2), but the exact order of events is unclear. Furthermore, although it has been proposed that Xic pairing may participate in monoallelic *Xist*/*Tsix* regulation (Nicodemi and Prisco, 2007), direct experimental evidence has never been provided in support of this model.

To assess patterns of *Xist*/*Tsix* expression before and after pairing in PGKT2-TetR cells, we first performed RNA FISH analysis on undifferentiated and day 1 differentiated cells. RNA FISH was performed using a combination of two double-stranded probes—one for *Tsix* (*DXPas34*), the other spanning 19 kb of *Xist* (p510) (Figure 5A). The p510 probe can detect both *Xist* and *Tsix* transcription, but we could distinguish *Xist*/*Tsix* RNA FISH profiles because the *DXPas34* probe is specific for *Tsix*, and because only *Xist* shows distinctive RNA "cloud" signals (Figure 5). Different categories of *Xist* and *Tsix* expression profiles were defined (Figures 5B and 5C). In undifferentiated ES cells, the overwhelming majority of cells showed biallelic *Xist* and *Tsix* expression (category 1, mauve) (Figures 5A–5D). At day 1 of differentiation, the proportion of cells showing different *Xist*/*Tsix* patterns increased as expected for the onset of XCI. In particular, a significant proportion of cells showed monoallelic *Tsix* and/or *Xist* expression (Figures 5B, 5C, and 5E). An increased proportion of cells (13.3%) also showed an accumulation of *Xist* RNA on one allele (category 2, pink; Figures 5B, 5C, and 5E). At this early stage, the *Xist* RNA clouds are much

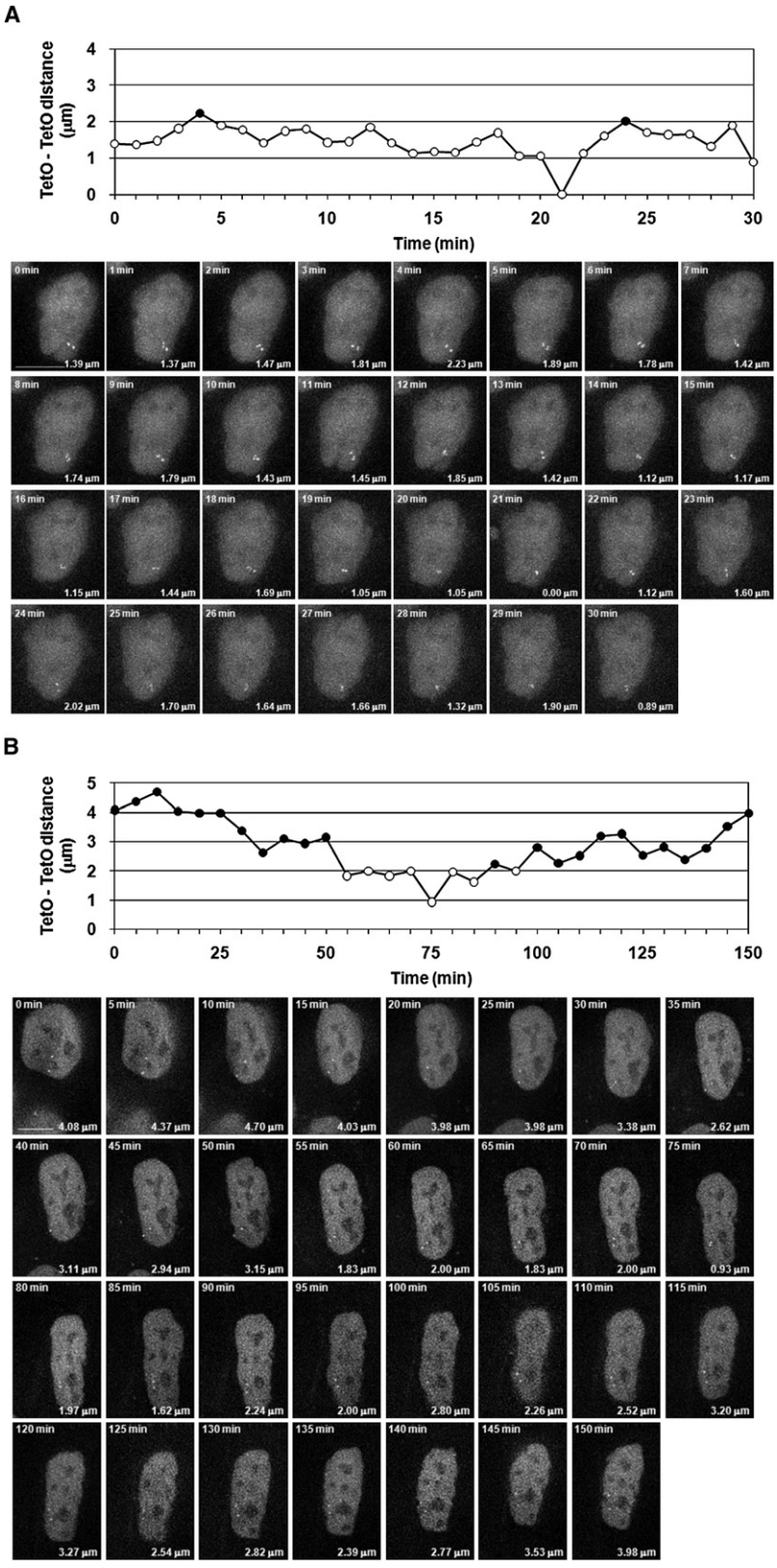

Figure 4. Time-Lapse Live-Cell Imaging of Xic Pairing Events in Early Differentiating ES Cells

(A) Representative snapshots of a day 1 differentiated PGKT2-TetR cell imaged over 30 min period at 1 min time intervals. Note that the two Xic^{TetO} loci show complete overlap at the 21 min time point. Open circles: Xic pairing ($d \leq 2$ μm). Scale bar = 10 μm. The whole movie is available as Movie S4.

(B) A representative image of a day 1 differentiated PGKT2-TetR cell imaged over 150 min at 5 min intervals. Note that the two Xic^{TetO} loci show pairing (≤ 2 μm, open circle) for 40 min (from the 55 min to the 95 min time points), and they show closest proximity at the 75 min time point. Scale bar = 10 μm. See also Movie S5.

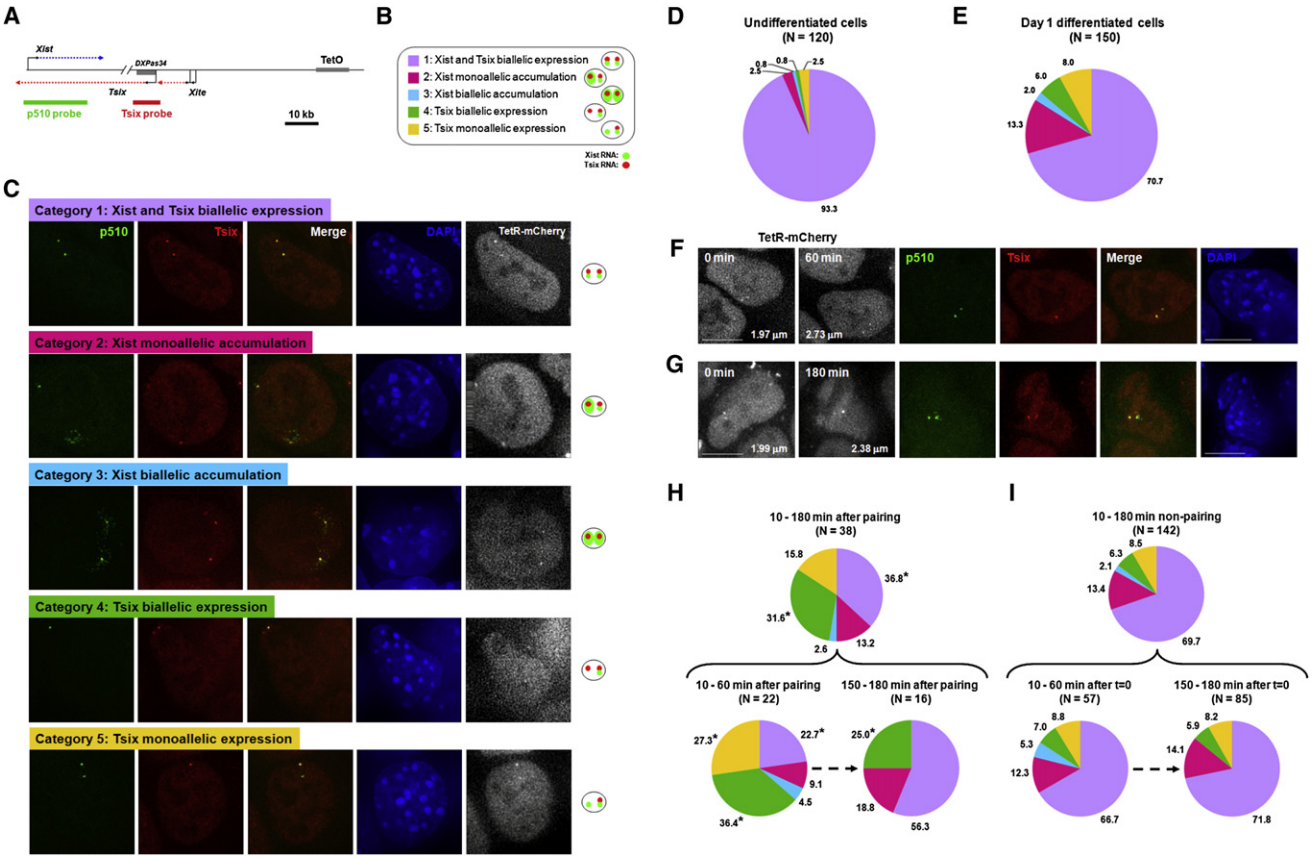

Figure 5. *Xist*/*Tsix* Expression Profiles and Their Link to Xic Pairing

(A) Schematic representation of the two probes used for RNA FISH. The p510 DNA probe covers most of the *Xist* gene and can detect both *Xist* and *Tsix* transcripts. The *Tsix* probe (*DXPas34*) covers the 5′ end of *Tsix* and detects only *Tsix* transcripts.

(B) Schematic representation of the five categories of RNA FISH signal patterns obtained for *Xist* and *Tsix* in undifferentiated and day 1 differentiated ES cells.

(C) Examples of the five categories of *Xist* and *Tsix* expression status. RNA FISH for *Xist*/*Tsix* (p510, green) and *Tsix* (red) are shown. Blue: DAPI. TetR-mCherry signal indicates the location of two Xic^{TetO} loci imaged in living cells prior to fixation and RNA FISH analysis.

(D) Distribution of the five categories of *Xist* and *Tsix* RNA FISH patterns in undifferentiated PGKT2-TetR cells.

(E) Distribution of the five categories of *Xist* and *Tsix* RNA FISH patterns in day 1 differentiated PGKT2-TetR cells.

(F) Representative nucleus showing *Tsix* monoallelic expression (category 5), 60 min following Xic pairing.

(G) Representative nucleus showing *Xist* RNA monoallelic accumulation (category 2), 180 min following Xic pairing. *Xist* RNA appears just upregulating.

(H) Distribution of *Xist*/*Tsix* RNA FISH patterns for all Xic pairing cells at day 1 differentiation (top); for Xic pairing cells 10 to 60 min after pairing at the beginning of the movie (t = 0) (left, bottom); and for Xic pairing cells 150 to 180 min after pairing at the beginning of the movie (t = 0) (right, bottom). *Category is statistically more significantly enriched when compared to nonpairing population (see also Tables S1A–S1C).

(I) Distribution of *Xist*/*Tsix* RNA FISH patterns for all Xic in cells at day 1 of differentiation that did not show pairing at the beginning of the movie (t = 0) (top); for cells 10 to 60 min after the beginning of the movie (left, bottom); and for cells 150 to 180 min after the beginning of the movie (right, bottom).

smaller and fainter than those observed in completely differentiated cells but nevertheless can clearly be distinguished from a punctate, nascent transcript signal. We also observed a small proportion of cells with biallelic *Xist* RNA clouds (category 3, blue; Figures 5B, 5C, and 5E).

Based on this fixed cell analysis, we concluded that asymmetric *Tsix* and *Xist* expression patterns are established during the same differentiation time window as Xic pairing. However, it remained unclear whether *Tsix* downregulation precedes or follows *Xist* upregulation, whether *Tsix* downregulation causes *Xist* upregulation, or whether *Xist* upregulation triggers *Tsix* silencing in *cis*, and whether any of these events are linked to Xic pairing. We therefore combined our live-cell imaging analysis of Xic pairing events with RNA FISH to evaluate the transcriptional output of *Xist* and *Tsix* and to define the temporal order of these different profiles relative to Xic pairing.

Live-cell imaging was performed as described above in undifferentiated and day 1 differentiated cells (Figure S2A) and immediately followed by fixation and RNA FISH using *Xist* and *Tsix* probes. Live-cell (TetR-mCherry) and RNA FISH data (3D stacks) were collected from the same cells. In differentiated cells, we examined *Xist*/*Tsix* expression status either at short (10–60 min) or long (150–180 min) intervals following the onset of live-cell imaging. Cells showing Xic pairing were considered to be those with Xic^{TetO} distances of ≤ 2 µm at the onset of time-lapse experiments. We observed that the proportion of

cells showing monoallelic *Tsix* expression (category 5, yellow) was higher in cells that had undergone pairing than in those that had not shown pairing (Figures 5E, 5H, and 5I; Table S1A). Moreover, monoallelic *Tsix* expression was found to be significantly enriched in cells at short (10–60 min) intervals after pairing, as compared to the cells that had not shown pairing ($p = 0.0083$) (Figures 5C, 5F, 5H, and 5I; Table S1B). The proportion of category 2 (pink) cells with monoallelic *Xist* RNA accumulation also increased after Xic pairing, but only at later intervals (150–180 min) after pairing (Figures 5C, 5G, and 5H; Table S1C). *Tsix*, on the other hand, had returned to a biallelic expression state (category 2) at these later time intervals when increased *Xist* RNA upregulation is seen (Figure 5G). Thus, *Tsix* expression on one of the two alleles is extinguished transiently after pairing (10–60 min), but the silent *Tsix* allele is re-expressed 1–2 hr later.

In summary, our findings combine real-time visualization of Xic pairing with analysis of *Xist*/*Tsix* expression status to define the precise order and potential causality of events at this critical decision-making time during XCI. We reveal dynamic changes in *Xist*/*Tsix* expression patterns following transient Xic interactions, with one of the two *Tsix* alleles being frequently silenced immediately (0–60 min) after pairing. The loss of *Tsix*-mediated repression on one allele may allow monoallelic *Xist* upregulation on that allele, as indicated by the increase in monoallelic *Xist* RNA accumulation observed subsequently (1–2 hr after pairing). By this time, however, the transiently silenced *Tsix* allele is re-expressed on the allele that has started to accumulate *Xist* RNA. Nevertheless, in cells that upregulate *Xist*, *Tsix* will eventually become silenced in *cis*. It should be noted that the transient *Tsix* asymmetry induced by Xic pairing may sometimes be unproductive as some cells revert to biallelic expression of *Tsix* with no *Xist* upregulation 1–2 hr later. However, as Xic pairing can occur not only at day 1 of differentiation but also at later time points (Augui et al., 2007; Xu et al., 2007), there would be an opportunity at the next cell cycle to establish an asymmetric *Tsix*/*Xist* expression profile. In conclusion, our findings demonstrate that *Tsix* pairing provides a potential window of opportunity for transient, asymmetric *Tsix* expression, which in turn could enable monoallelic *Xist* upregulation in *cis* and could thus be a key event in the choice step during XCI initiation.

DISCUSSION

Inter- and intrachromosomal interactions in the nucleus have been increasingly linked to gene regulation and/or the coordination of gene expression (for reviews see Williams et al., 2010 and Schoenfelder et al., 2010). Knowledge of the exact outcome of such *trans*-associations, at the level of gene expression, has been lacking, however, as studies so far were performed only in fixed cells, which can only provide snapshots and do not allow precise ordering of dynamic events. Here, we describe the in vivo dynamics and outcome of homologous *trans*-interactions that occur between the two *Tsix* loci on X chromosomes during the initiation of XCI in differentiating female ES cells. This study provides one of the first in vivo spatiotemporal analyses of chromosomal dynamics and homologous chromosomal interactions in ES cells. Our data support the hypothesis that pairing at the Xic loci can facilitate the establishment of asymmetric expression patterns. We also demonstrate that such events occur in the context of increasing genome dynamics during early differentiation. Live-cell imaging of the Xics and of other, autosomal loci that we present here provides important insights into locus mobility in ES cells and their early differentiated derivatives. The mobility of loci that we found in undifferentiated ES cells ($\sim$0.01 μm^2/min) is in fact similar to values previously observed for loci in transformed human cell lines ($\sim$0.008 μm^2/min) (Chubb et al., 2002). The motion we detected for the Xic loci in ES cells corresponded to constrained diffusion, with a radius of constraint of $\sim$1.7 μm, which could correspond to the degree of constraint in a chromosome territory. Indeed, the Xic has been previously shown not to loop out of its territory to any significant extent (Augui et al., 2007). In the course of our analyses, we observed no signs of significant directional long-range movements, such as those described following induction by transcriptional activators in somatic cells (Chuang et al., 2006). However, we did find an increase in locus mobility during early differentiation. The mobility reached after 1–3 days of differentiation approximates to the "rapid" motion observed following induction of specific loci by transcriptional activators (Chuang et al., 2006). This increase in locus mobility may be a general characteristic of the early differentiating ES cell genome, as we observed a similar increase for all loci examined. Intriguingly, chromatin dynamics (histone exchange) has been reported to decrease during differentiation of ES cells (Meshorer et al., 2006). However, chromosome dynamics, which is a different (though possibly related) phenomenon than chromatin dynamics, had not so far been evaluated. Our results open up the possibility that increasing dynamics of genomic loci may accompany, or even participate in, the changes in gene activity underlying lineage-specific decisions in differentiating ES cells. This would be consistent with the recent proposal that chromosome position and configuration change during differentiation (Rajapakse et al., 2009). The increased mobility of genomic loci that we have detected may reflect active chromatin-remodeling movements within the nucleus, as has been reported in yeast nuclei (Gartenberg et al., 2004), and/or be symptomatic of increased cytoskeletal movements, which could impose movement and deformation on the nuclear envelope and its contents.

Whatever the underlying cause of increased Xic mobility during early differentiation, we believe that this might facilitate the onset of pairing by increasing the frequency of collisions between loci and/or with different nuclear compartments (Figure 6). However, once they have collided, the Xic loci remain tethered to each other (or to a specific nuclear compartment) as there is a marked decrease in mobility during pairing. Such tethering could occur via specific sequences in the Xic, or via association with a common nuclear compartment. So far, none of the nuclear compartments we have examined, such as nucleoli, the nuclear envelope, or replication foci, appear to be specific sites of Xic pairing (Bacher et al., 2006; Augui et al., 2007; and O.M., N.M., and E.H., unpublished data). Although DNA-binding factors, such as CTCF and Oct4, have been implicated in pairing (Xu et al., 2007; Donohoe et al., 2009), the ubiquitous nature of their binding is unlikely to explain the specificity of Xic pairing. Xic elements such as the *Xpr* locus may facilitate such specificity. Unlike *Tsix*, *Xpr* can pair autonomously

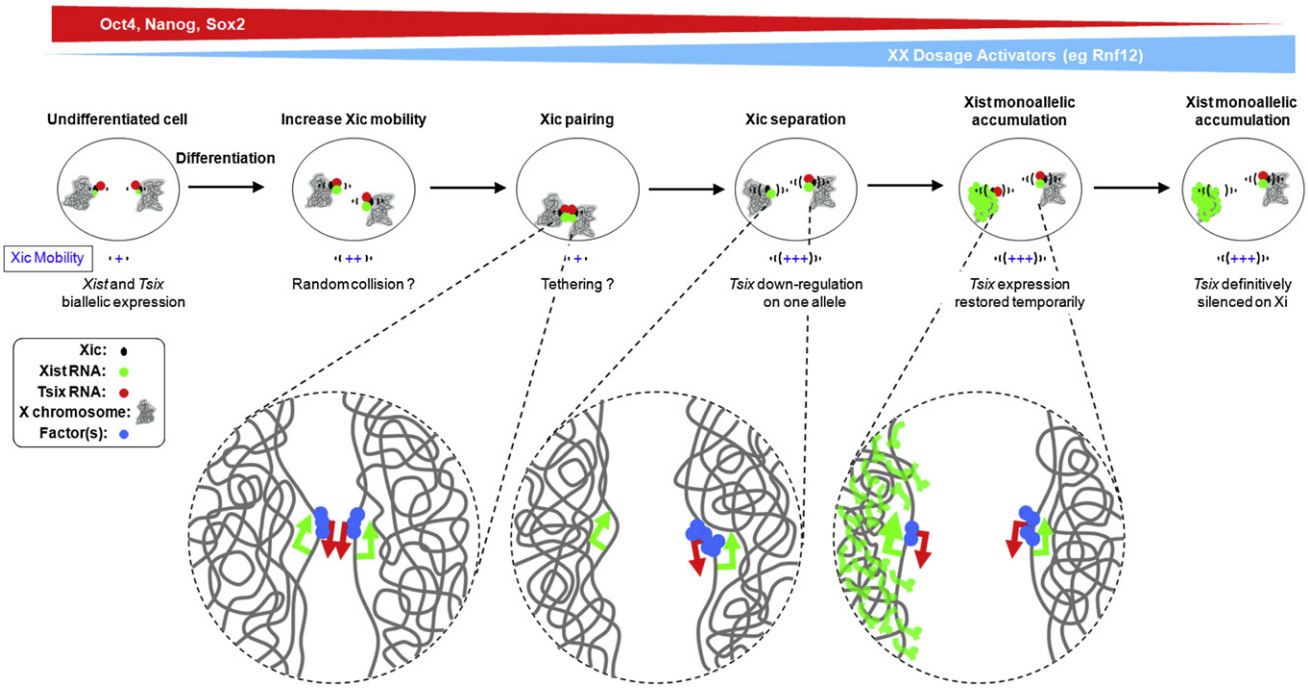

Figure 6. Model for Monoallelic *Tsix* and *Xist* Regulation downstream of Pairing at *Tsix/Xite*

From left, nucleus of an undifferentiated ES cell, where both the X chromosomes are actively transcribed and *Tsix* is biallelically expressed, *Xist* being more weakly expressed. Upon differentiation, the mobility of chromosomes increases; this may result in increased frequency of random collisions between the two Xic loci. Once the two loci come together, they stay in close proximity ($d \leq 2$ μm) for ~45 min and display reduced mobility, indicative of possible tethering to each other, either directly or via some common nuclear compartment. Immediately after pairing, *Tsix* expression becomes monoallelic transiently, through asymmetric distribution of certain factor(s) at the locus (schematically shown below). This transient downregulation of *Tsix* can provide an opportunity for upregulation of *Xist* transcription in *cis* and thus initiate XCI. *Tsix* monoallelic expression may return to a biallelic pattern at later time points, but this will no longer be able to prevent *Xist* RNA accumulation, and ultimately *Tsix* will be silenced by *Xist* in *cis*, ensuring that asymmetric *Xist* expression is locked in.

when present as a single-copy transgene (Bacher et al., 2006; Augui et al., 2007). Furthermore, *Xpr* is part of a large H3K9me2/H3K27me3 hotspot (Heard et al., 2001) that may help to hold the Xic loci together via heterochromatic proteins, thus enabling the *Tsix* loci to interact, with the help of proteins such as CTCF and Oct4. Keeping the loci together for a prolonged period of approximately 45 min may be essential for the exchange of information that occurs during Xic pairing and for its subsequent outcome.

Our findings shed new light on the outcome of pairing as we show that after the two *Tsix* loci have spent time in close proximity, they frequently show asymmetric expression upon separation. The explanation we favor is that during pairing, one or more regulatory factors of *Tsix* becomes asymmetrically distributed, resulting in unequal transcription on the two alleles during the 10–60 min time window following their separation (Figure 6). Although CTCF and Oct4, which are both reported to bind *Tsix/Xite*, are candidates for these regulatory factors, so far no evidence has shown that they become asymmetric (Xu et al., 2007; Donohoe et al., 2009). The fact that, after just 1 hr, *Tsix* biallelic expression is restored implies that asymmetry is transient. Nevertheless, by this time *Xist* upregulation has begun in an increased number of cells. We propose that the transient asymmetry in *Tsix* expression initiated during pairing creates a window of opportunity for upregulation of the *Xist* allele that is associated with the transiently downregulated *Tsix* allele. Once *Xist* RNA starts to accumulate, it will then presumably silence *Tsix* in *cis*. Thus a negative feedback loop is established, whereby transient, monoallelic downregulation of *Tsix* enables the upregulation of *Xist*, which will then shut down *Tsix* and lock in the transient asymmetry created by pairing (Figure 6). Although *Tsix* reverts to biallelic expression without *Xist* RNA accumulation in some cases, Xic pairing during subsequent cell cycles could allow other opportunities for *Tsix/Xist* expression symmetry to be broken productively. We believe that this mechanism of *Xist* symmetry breaking via the *Tsix* locus could be a mechanism that evolved to optimize monoallelic *Xist* regulation in the mouse, as an additional layer of regulation to stochastic events and feedback loops provided by X-linked activators such as Rnf12 (Jonkers et al., 2009). Indeed, in other mammals such as humans and rabbits, where a functional *Tsix* homolog may not exist, substantial biallelic *Xist* upregulation can be found during initiation of XCI (Okamoto et al., 2011). In these mammals, *Xist* expression may ultimately become monoallelic only as a result of stochastic events, Rnf12-like feedback loops, and/or counterselection (Monkhorst et al., 2008).

In conclusion, our study reveals the in vivo dynamics of chromosomal *trans*-interactions during early differentiation and shows that pairing can result in transiently asymmetric gene expression between two alleles. Defining the nature of the factors involved in Xic tethering and pairing, as well as those

that are exchanged and become transiently asymmetrically distributed after pairing has occurred, represents the next challenge. It will also be of interest to assess the degree to which *trans*-interactions participate in establishing asymmetric gene expression at loci other than the Xic, both in the context of random monoallelic gene expression (for review, see Ohlsson, 2007), as well as for nonhomologous loci when developmental decisions are being taken, and mutually exclusive expression patterns may sometimes be required.

EXPERIMENTAL PROCEDURES

Cell Culture

Feeder-independent PGK12.1 mouse female ES cells were a gift from Neil Brockdorff (Penny et al., 1996), and their culture has previously been described in detail (Bacher et al., 2006; Augui et al., 2007). Briefly, ES cells were cultured in DMEM with 15% FCS, 1000 U/ml LIF, and Penicillin-Streptomycin (GIBCO) in 8% CO_2. ES cells were grown on gelatin-coated glass coverslips. Differentiation was induced in the presence of all-*trans*-retinoic acid, as described previously (Rougeulle et al., 2004).

Plasmids and Constructs

To generate a targeting plasmid pSPO2/FAB/TetO for homologous recombination, two homology arms were PCR-amplified from mouse genomic DNA with the primers (FA arm primers, 169 and 4756B; FB arm primers, 4756A and 910B) as previously described (Clerc and Avner, 1998) and inserted into the pSPO2 plasmid. The primer sequences are as follows: 169, 5′-CATGAGCTTTGCATCTAGGG-3′; 4756B, 5′-TGCCAGGACTTTGGAACA-3′; 4756A, 5′-CAAAGCCACACGGTTCAA-3′; 910B, 5′-ATTCAACTGCAAGTGAAT-3′. Two hundred and twenty-four copies of a TetO DNA array and Neomycin-resistant cassette flanked with *loxP* sequences were inserted between two homologous arms. Plasmids were amplified with MaxStbl2-competent *E. coli* (Invitrogen). N-terminal of mCherry open reading frame (ORF) was fused with the C-terminal of TetR ORF on pBluescript plasmid (Stratagene), then the c-Myc NLS sequence was inserted between two ORFs to generate TetR-NLS-mCherry ORF. The TetR-NLS-mCherry ORF was inserted into the pBROAD3 expression plasmid (Invivogen) to generate pBROAD3/TetR-mycNLS-mCherry. mCherry cDNA was a gift from Roger Tsien.

Gene Targeting and Southern Blotting

PGK12.1 cells were electroporated with NotI-linearized pSPO2/FAB/TetO plasmid and selected with Neomycin (0.3 mg/ml). Colonies were picked and screened by Southern blotting, using standard protocols. Briefly, extracted genomic DNA was digested with PstI, then resolved on a 0.6% agarose gel. The resolved DNA was transfered to Positive TM Membrane (Qbiogen) and probed with ^{32}P-labeled FD-1/2 DNA probe (generated with PCR primers FD1 and FD2) to distinguish wild-type (WT) allele and targeted allele. The primer sequences are as follows: FD1, 5′-GCCAGGGTTGGGTCTTGAAC-3′; FD2, 5′-CCGACCCGACTGAGGAGTTT-3′.

In order to generate homozygous Xic^{TetO} cells, one of the heterozygous Xic^{TetO} clones identified was treated with increased dosage of G418 (30 mg/ml) for 1 week. Colonies were picked and assessed by Southern blotting for the presence of the targeted allele but the absence of the WT allele. Clones were further analyzed by DNA FISH on metaphase spreads to confirm karyotype, $Xic^{TetO}Xic^{TetO}$ status, and chromosome integrity. The pBROAD3/TetR-mycNLS-mCherry-expressing construct was transfected into PGKT2 cells and selected with Hygromycin B, using standard transfection and selection procedures (see Augui et al., 2007).

Live-Cell Imaging

PGKT2 cells expressing the TetR-mCherry transgene were seeded at 5×10^4 cells/cm^2 on gridded-glass-bottom dishes (Matsunami Inc.) or on 12 mm coverslips in a 6-well plate for 1 or 2 days before differentiation was initiated. All images were acquired with 60 ms exposure time and 100×/1.4 objective with 0.3 μm intervals between planes by the DeltaVision system (API). Total exposure time was kept less than 100 s to avoid excess phototoxicity. All images were deconvolved and analyzed with softWoRx software (API). Toxicity was assessed using various conditions of imaging and by assessing cell morphology and viability after several hours.

Mean Square Displacement Analysis

Three-dimensional manual tracking of distance between the two loci was performed using the "measure distance" tool in softWoRx software. MSD calculation was carried out using Matlab (mathworks, http://www.mathworks.com/). Assuming that chromatin motion is modeled as a random walk (Marshall et al., 1997), the relative mobility of the loci can be determined by plotting their mean square displacement (MSD or $< \Delta d^2 >$ where $\Delta d = d(t+\Delta t)-d(t)$) as a function of increasing time intervals Δt (d is the distance between the two loci at each time point). Free diffusion (unconstrained motion) gives a linear relationship between MSD and time intervals, whereas in the case of constrained diffusion, the MSD will reach a "plateau." According to Qian et al. (1991), the statistical errors related to MSD computation quickly become large when Δt becomes large: as a result, MSD curves should be based only on early time points (the first quarter of all time points). Error bars in individual MSD curves were calculated using the appropriate statistical approach (Saxton, 1997). Slopes k of individual MSD curves were obtained by a least-square linear fitting of the first quarter of points. Three-dimensional diffusion constant D were then determined $k = 6D$, as our analyses were done in 3D. To make the analysis more robust (i.e., to circumvent the statistical variance inherent to individual cells), we averaged all individual MSDs over all the individual runs recorded for a given differentiation stage. After averaging over N individuals' MSDs, the error bar is thus reduced by a factor of about $1/\sqrt{N}$.

Immunofluorescence and RNA and DNA FISH

Immunofluorescence, RNA FISH, and DNA FISH were performed as described previously (http://www.epigenome-noe.net/WWW/researchtools/protocol.php?protid=3 and Augui et al., 2007). The *Xist* probe was the p510 plasmid (Rougeulle et al., 1994) and the *Tsix* probe was the *DXPas34* plasmid (Debrand et al., 1999). The bacterial artificial chromosomes (BACs) used as probes for certain regions of Xic were as described previously (Augui et al., 2007).

SUPPLEMENTAL INFORMATION

Supplemental Information includes Extended Experimental Procedures, four figures, one table, and five movies and can be found with this article online at doi:10.1016/j.cell.2011.03.032.

ACKNOWLEDGMENTS

We thank members of the Heard laboratory and John Sedat for helpful discussions; Michèle Guggiari, Christel Picard, Matt Plutz, and Patricia Diabangouaya for technical assistance; Yohanns Bellaiche, François Graner, and Jennifer Chow for helpful advice and for critical reading of the manuscript. We thank Olivier Renaud and Olivier Leroy (PICT@BDD imaging facility), as well as Sebastian Huart for assistance with image analysis. This work was supported by the Human Frontier Science Program to E.H. and A.S.B.; the EU FP7 program HEROIC IP; ANR and FRM funding, and an ERC Advanced Investigator Award to E.H.; and the FRM to I. Bonnet (postdoc grant n° SPF20080512397).

Received: November 5, 2010
Revised: February 23, 2011
Accepted: March 18, 2011
Published: April 28, 2011

REFERENCES

Augui, S., Filion, G.J., Huart, S., Nora, E., Guggiari, M., Maresca, M., Stewart, A.F., and Heard, E. (2007). Sensing X chromosome pairs before X inactivation via a novel X-pairing region of the Xic. Science *318*, 1632–1636.

Bacher, C.P., Guggiari, M., Brors, B., Augui, S., Clerc, P., Avner, P., Eils, R., and Heard, E. (2006). Transient colocalization of X-inactivation centres accompanies the initiation of X inactivation. Nat. Cell Biol. *8*, 293–299.

Carmo-Fonseca, M., Platani, M., and Swedlow, J.R. (2002). Macromolecular mobility inside the cell nucleus. Trends Cell Biol. *12*, 491–495.

Chuang, C.H., Carpenter, A.E., Fuchsova, B., Johnson, T., de Lanerolle, P., and Belmont, A.S. (2006). Long-range directional movement of an interphase chromosome site. Curr. Biol. *16*, 825–831.

Chubb, J.R., Boyle, S., Perry, P., and Bickmore, W.A. (2002). Chromatin motion is constrained by association with nuclear compartments in human cells. Curr. Biol. *12*, 439–445.

Chureau, C., Chantalat, S., Romito, A., Galvani, A., Duret, L., Avner, P., and Rougeulle, C. (2011). Ftx is a non-coding RNA which affects *Xist* expression and chromatin structure within the X-inactivation center region. Hum. Mol. Genet. *20*, 705–718.

Clerc, P., and Avner, P. (1998). Role of the region 3′ to *Xist* exon 6 in the counting process of X-chromosome inactivation. Nat. Genet. *19*, 249–253.

Debrand, E., Chureau, C., Arnaud, D., Avner, P., and Heard, E. (1999). Functional analysis of the *DXPas34* locus, a 3′ regulator of *Xist* expression. Mol. Cell. Biol. *19*, 8513–8525.

Donohoe, M.E., Silva, S.S., Pinter, S.F., Xu, N., and Lee, J.T. (2009). The pluripotency factor Oct4 interacts with Ctcf and also controls X-chromosome pairing and counting. Nature *460*, 128–132.

Gartenberg, M.R., Neumann, F.R., Laroche, T., Blaszczyk, M., and Gasser, S.M. (2004). Sir-mediated repression can occur independently of chromosomal and subnuclear contexts. Cell *119*, 955–967.

Gimelbrant, A., Hutchinson, J.N., Thompson, B.R., and Chess, A. (2007). Widespread monoallelic expression on human autosomes. Science *318*, 1136–1140.

Heard, E., Rougeulle, C., Arnaud, D., Avner, P., Allis, C.D., and Spector, D.L. (2001). Methylation of histone H3 at Lys-9 is an early mark on the X chromosome during X inactivation. Cell *107*, 727–738.

Hewitt, S.L., Yin, B., Ji, Y., Chaumeil, J., Marszalek, K., Tenthorey, J., Salvagiotto, G., Steinel, N., Ramsey, L.B., Ghysdael, J., et al. (2009). RAG-1 and ATM coordinate monoallelic recombination and nuclear positioning of immunoglobulin loci. Nat. Immunol. *10*, 655–664.

Jonkers, I., Barakat, T.S., Achame, E.M., Monkhorst, K., Kenter, A., Rentmeester, E., Grosveld, F., Grootegoed, J.A., and Gribnau, J. (2009). RNF12 is an X-encoded dose-dependent activator of X chromosome inactivation. Cell *139*, 999–1011.

Lee, J.T. (2005). Regulation of X-chromosome counting by *Tsix* and *Xite* sequences. Science *309*, 768–771.

Lee, J.T., and Lu, N. (1999). Targeted mutagenesis of *Tsix* leads to nonrandom X inactivation. Cell *99*, 47–57.

Lee, J.T., Davidow, L.S., and Warshawsky, D. (1999). *Tsix*, a gene antisense to Xist at the X-inactivation centre. Nat. Genet. *21*, 400–404.

Lyon, M.F. (1961). Gene action in the X-chromosome of the mouse (Mus musculus L.). Nature *190*, 372–373.

Marshall, W.F., Straight, A., Marko, J.F., Swedlow, J., Dernburg, A., Belmont, A., Murray, A.W., Agard, D.A., and Sedat, J.W. (1997). Interphase chromosomes undergo constrained diffusional motion in living cells. Curr. Biol. *7*, 930–939.

Meshorer, E., Yellajoshula, D., George, E., Scambler, P.J., Brown, D.T., and Misteli, T. (2006). Hyperdynamic plasticity of chromatin proteins in pluripotent embryonic stem cells. Dev. Cell *10*, 105–116.

Michaelis, C., Ciosk, R., and Nasmyth, K. (1997). Cohesins: chromosomal proteins that prevent premature separation of sister chromatids. Cell *91*, 35–45.

Monkhorst, K., Jonkers, I., Rentmeester, E., Grosveld, F., and Gribnau, J. (2008). X inactivation counting and choice is a stochastic process: evidence for involvement of an X-linked activator. Cell *132*, 410–421.

Mortensen, R.M., Conner, D.A., Chao, S., Geisterfer-Lowrance, A.A., and Seidman, J.G. (1992). Production of homozygous mutant ES cells with a single targeting construct. Mol. Cell. Biol. *12*, 2391–2395.

Navarro, P., and Avner, P. (2010). An embryonic story: analysis of the gene regulative network controlling *Xist* expression in mouse embryonic stem cells. Bioessays *32*, 581–588.

Navarro, P., Chambers, I., Karwacki-Neisius, V., Chureau, C., Morey, C., Rougeulle, C., and Avner, P. (2008). Molecular coupling of Xist regulation and pluripotency. Science *321*, 1693–1695.

Nicodemi, M., and Prisco, A. (2007). Symmetry-breaking model for X-chromosome inactivation. Phys. Rev. Lett. *98*, 108104–108114.

Ogawa, Y., and Lee, J.T. (2003). *Xite* X-inactivation intergenic transcription elements that regulate the probability of choice. Mol. Cell *11*, 731–743.

Ohlsson, R. (2007). Genetics. Widespread monoallelic expression. Science *318*, 1077–1078.

Okamoto, I., and Heard, E. (2009). Lessons from comparative analysis of X-chromosome inactivation in mammals. Chromosome Res. *17*, 659–669.

Okamoto, I., Patrat, C., Thepot, D., Peynot, N., Fauque, P., Daniel, N., Diabangouya, P., Wolf, J.P., Renard, J.P., Duranthon, V., and Heard, E. (2011). Eutherian mammals use diverse strategies to initiate X-chromosome inactivation during development. Nature. Published online April 6 2011. 10.1038/nature09872.

Penny, G.D., Kay, G.F., Sheardown, S.A., Rastan, S., and Brockdorff, N. (1996). Requirement for *Xist* in X chromosome inactivation. Nature *379*, 131–137.

Qian, H., Sheetz, M.P., and Elson, E.L. (1991). Single particle tracking. Analysis of diffusion and flow in two-dimensional systems. Biophys. J. *60*, 910–921.

Rajapakse, I., Perlman, M.D., Scalzo, D., Kooperberg, C., Groudine, M., and Kosak, S.T. (2009). The emergence of lineage-specific chromosomal topologies from coordinate gene regulation. Proc. Natl. Acad. Sci. USA *106*, 6679–6684.

Rougeulle, C., Colleaux, L., Dujon, B., and Avner, P. (1994). Generation and characterization of an ordered lambda clone array for the 460-kb region surrounding the murine Xist sequence. Mamm. Genome *5*, 416–423.

Rougeulle, C., Chaumeil, J., Sarma, K., Allis, C.D., Reinberg, D., Avner, P., and Heard, E. (2004). Differential histone H3 Lys-9 and Lys-27 methylation profiles on the X chromosome. Mol. Cell. Biol. *24*, 5475–5484.

Sado, T., Wang, Z., Sasaki, H., and Li, E. (2001). Regulation of imprinted X-chromosome inactivation in mice by Tsix. Development *128*, 1275–1286.

Saxton, M.J. (1997). Single-particle tracking: the distribution of diffusion coefficients. Biophys. J. *72*, 1744–1753.

Schoenfelder, S., Clay, I., and Fraser, P. (2010). The transcriptional interactome: gene expression in 3D. Curr. Opin. Genet. Dev. *20*, 127–133.

Scialdone, A., and Nicodemi, M. (2008). Mechanics and dynamics of X-chromosome pairing at X inactivation. PLoS Comput. Biol. *4*, e1000244.

Sun, B.K., Deaton, A.M., and Lee, J.T. (2006). A transient heterochromatic state in *Xist* preempts X inactivation choice without RNA stabilization. Mol. Cell *21*, 617–628.

Tian, D., Sun, S., and Lee, J.T. (2010). The long noncoding RNA, *Jpx* is a molecular switch for X chromosome inactivation. Cell *143*, 390–403.

Williams, A., Spilianakis, C.G., and Flavell, R.A. (2010). Interchromosomal association and gene regulation in *trans*. Trends Genet. *26*, 188–197.

Xu, N., Tsai, C.L., and Lee, J.T. (2006). Transient homologous chromosome pairing marks the onset of X inactivation. Science *311*, 1149–1152.

Xu, N., Donohoe, M.E., Silva, S.S., and Lee, J.T. (2007). Evidence that homologous X-chromosome pairing requires transcription and Ctcf protein. Nat. Genet. *39*, 1390–1396.